APWEN Journal of Engineering, Science and Technology
ISSN: 2714-2396, Volume 7 Issue 1

IMAGE COMPRESSION SCHEME USING COMBINED WALSH-HADAMARD AND BI-ORTHOGONAL DISCRETE WAVELET TRANSFORM

A.K. Ojetunde[1], K.A. Amusa[1], O.O. Nuga[1] and M.T. Raji[2]

[1]Department of Electrical and Electronics Engineering, Federal University of Agriculture, Abeokuta, Nigeria
[2]Department of Mathematics, Federal University of Agriculture, Abeokuta, Nigeria
adexd1@yahoo.com; amusaka@funaab.edu.ng; nugaoo@funaab.edu.ng; rajimt@funaab.edu.ng
adexd1@yahoo.com (Corresponding author)

Received Date: 2nd May 2024 Accepted Date 16th July 2024 Published Date:15th Sept., 2024

ABSTRACT
This study presents a compression scheme (CS) for still images using combined Walsh-Hadamard (WH) and bi-orthogonal discrete wavelet (BDW) transforms. The developed compression scheme is formulated using a combined WH transform of order 2 and fifteen randomly selected BDW transforms with a decomposition level 2. The selected fifteen BDWs are 'bior1.1', 'bior1.3', 'bior1.5', 'bior2.2', 'bior2.4', 'bior2.6', 'bior2.8', 'bior3.1', 'bior3.3', 'bior3.5', 'bior3.7', 'bior3.9', 'bior4.4', 'bior5.5', and 'bior6.8'. The implementation was done in MATLAB R2018a environment. Compression ratio (CR), mean square error (MSE) and peak signal-to-noise ratio (PSNR) were used as evaluation metrics. A CS is adjudged best with an above-average CR value, the lowest MSE, and the highest PSNR. Nine different images of different sizes are used for evaluation. The CSs involving bior2.2, bior2.4, bior4.4, bior5.5 and bior6.8 satisfied the CR criterion. The lowest MSE and highest PSNR figures were recorded for images 1, 4, 5, 7, 8 and 9 when bior2.2 was used, while bior2.4 gave the lowest MSE and highest PSNR values for images 2, 3 and 6. Implementations involving bior2.4 had advantages of 0.64%, 1.97% and 12.20% over bior2.2 for images 2, 3 and 6, respectively, in terms of MSE, while corresponding PSNR advantages were 0.04%, 0.12% and 0.71%. Thus, it can be said without loss of generality that implementation employing bior2.2 is better than that utilizing bior2.4 based on computed MSE and PSNR values. Thus, a compression scheme formulated with a combined Walsh-Hadamard transform and bior2.2 variant of discrete wavelet transform is the best suited for still image compression.
Keywords: compression scheme, still image, bi-orthogonal discrete wavelet transform, Walsh-Hadamard transform

1. INTRODUCTION
In this modern age of massive data, the size of the data is of growing concern for researchers and scientists dealing with such data. The constraints of transmission channel bandwidth and storage space, which are limited, call for data compression while in transit as well as for archiving without compromising integrity [1]. Data come in different forms, such as sound, picture, video, and text documents. Each of these forms of data requires a sort of compression to ensure efficient utilization of transmission resources and available memory space for storage. Uncompressed data occupy much space in the computer's random-access memory and storage media; it also takes more time to exchange between devices. When rendered in digital format, an image is either a two-dimensional signal (if it is a grayscale) or three-dimensional (if it is a

coloured image). Usually, an image is taken via a camera and comes in the traditional analogue format. However, images are changed into digital equivalents for processing, which may involve transmission and storage. A digital image is described as a group of pixels [2]. Varieties of images are encountered in day-to-day activities and specialized engagements such as remote sensing, bio-medical, exploration, and entertainment. Images are often processed, and compression is included before transmission and storage. A typical digital image contains three components: useful, redundant, and irrelevant. While the irrelevant component can be done away with through the compression of an image, the redundant information is vital for highlighting the image details. The useful component is neither redundant nor irrelevant and must not be tampered with to avoid compromising the integrity of the image. Without accurate, useful image information, reconstruction of the original image via decompression results in an unsatisfactory output [3].

In other words, image compression is realized by removing the whole of irrelevant and calculated amount of redundant bits from the image. This makes the image's compression different from that of any other digital data. Consequently, performances of general-purpose data compression schemes are often less than optimal when adopted for image compression tasks. Image compression approaches can generally be grouped into two, just like any other data compression type. Image compression schemes could be considered lossy or lossless, depending on the degree of post-compression distortion introduced into the image. At the same time, the lossless procedure yields an output image that, when decompressed, produces an exact copy of the uncompressed image. A lossy method introduces a certain amount of error in the compressed image. In addition, there are small savings in transmission bandwidth and space for storage using lossless techniques, unlike lossy schemes that are characterized by increased compression performance, although at the price of losing few image details. A few approaches for lossless image compression are bit-plane coding, Shannon-Fano coding, Lempel-Ziv-Welch coding, entropy coding, Huffman coding, run-length coding, and arithmetic coding, among others. Examples of lossy compression methods are transform coding (Fourier, discrete cosine, discrete sine, and wavelet) and fractal compression. While lossless approaches are efficient for small data, the lossy methods find applications in areas such as TV broadcast, video conferencing, and facsimile transmission, each of which involves large data [2].

Image compression is considered efficient when the amount of data needed for representation and storage space for an image is minimal. These are in addition to increased transfer efficiency. The need for an efficient image compression method has led to different proposals in the literature. A few of such efforts include that of combined wavelet transform and run-length encoding [4], singular value decomposition (SVD) method [5], non-negative matrix factorization (NMF) based image compression approach [6], matrix-based method with thresholding and value diminution [7], bit-rate coding model for predictive coding [8], combined move-to-front transformations, Burrows-Wheeler transform, run length and arithmetic encoding approaches [9], compressed adaptive integration scheme (C-AIS) [10], compressing dense media descriptors technique [11], combined Frei-Chen bases and the run length method [12], spatial orientation block trees-based technique [13], neural network-based technique [14], wavelet-based method [15], binary multi-level quantization arithmetic coding utilizing a look-up table [16], and fractal characteristics based method [17].

Judging from various surveys reported, it is obvious that lossless compression approaches are less appropriate for images, as much of the image's detail can be done away with, without monumental damage to the image's appearance. This is typically the case with non-medical images. For medical images (CT scan, MRI scan, ultrasound, X-ray etc.) there is hardly room for elimination of image’s details without compromising the essence of such images. Where lossy compression method is employed, the image size is drastically reduced at the expense of losing very fine details of the image. To ensure satisfactory results, several performance indices, including peak-signal-to-noise-ratio and mean square error, are often utilized to assess the compression technique in terms of the disparity between the reconstructed image produced from decompression and the initial (uncompressed) image. This research is concerned with developing a still image compression scheme using combined bi-orthogonal discrete wavelet, and Walsh-Hadamard transforms. The research is motivated by the fact that multimedia data nowadays requires large storage coupled with ubiquitous mobile devices with inherently limited storage and transmission capacities. There is therefore the need for a compression scheme that has relatively higher compression ratio of acceptable error. Each of biorthogonal discrete wavelet transform and Walsh-Hadamard transform is individually effective as lossy image compression technique with a high compression ratio. Combining the two in a compression scheme formulaton is might result in a higher compression ratio.

2. THEORETICAL BACKGROUND

The theoretical basis of the two transforms employed in developing compression schemes for still images presented in this study are briefly discussed in this section. This is began with wavelet transform.

2.1 Wavelet Transform

Mathematically, a wavelet can be described as any function $\psi(t) \in L^2(R)$ where $L^2(R)$ is a space that encloses functions that are square-integrable on the set of real numbers R. The necessary and sufficient condition for $\psi(t)$ to occur is $\widehat{\psi}(t) = 0$, indicating that:

$$\int_{-\infty}^{\infty} \psi(t)\, dt = 0 \quad (1)$$

The implication of (1) is that all zero-integral functions constitute wavelets. Wavelets are usually obtained from the mother wavelet via wavelet parameters, which include scaling (dilating) and translating parameters.

Supposing $\psi(t)$ represents the mother wavelet while the scaling and translating parameters are given by a and b, respectively, the wavelet basis $\psi_{a,b}(t)$ is expressible as:

$$\psi_{a,b}(t) = \left(\sqrt{a}\right)^{-1} \psi\left[(t-b)a^{-1}\right] \quad (2)$$

where a and b are real numbers with $a \neq 0$ and; $\left(\sqrt{a}\right)^{-1}$ is a normalization factor to guarantee that the transformed signal exhibits equal energy at every scale; and t indicates time.

When all entities (input signal values, scaling and translating parameters) involved in wavelet transform assume discrete values, the resultant wavelet transform is called discrete wavelet transform (DWT). The DWT can be expressed as follows [18]:

$$c_{j,k} = \sum_{n=-\infty}^{\infty} x(n)\, \Phi_{j,k}(n) \quad (3)$$

and,

$$d_{j,k} = \sum_{n=-\infty}^{\infty} x(n)\,\psi_{j,k}(n) \tag{4}$$

provided $c_{j,k}$ represents the approximated coefficient; $d_{j,k}$ stands for the detailed coefficients; $j,k \in Z$, Z are set of positive integers; $x(n)$ and $\Phi(n)$ are the input discrete signal and scaling function, respectively, such that:

$$\Phi_{j,k}(n) = \sqrt{2^j}\,\Phi\left(2n-k\right) \tag{5}$$

and $\psi(n)$ constitutes the mother wavelet, which permits

$$\psi_{j,k}(n) = \sqrt{2^j}\,\psi\left(2n-k\right) \tag{6}$$

Inverse wavelet transform which is defined by

$$x(n) = \sum_{k=-\infty}^{\infty} c_{l,k}\Phi_{l,k}(n) + \sum_{j=l}^{\infty}\sum_{k=-\infty}^{\infty} d_{j,k}\psi_{j,k}(n) \tag{7}$$

is used to retrieve the original signal $x(n)$ from the transformed wavelets. In (7), l is the decomposition level used in the wavelet transformation while other symbols assume earlier definitions.

In this study, bi-orthogonal functions mother wavelets are utilized. Bi-orthogonal wavelets represent a class of compactly supported symmetric wavelets that are characterized by two scaling functions. Bi-orthogonal wavelets lend themselves to different multi-resolution analysis which results in two distinct wavelet functions. Additional information and necessary conditions on the realization of this class of wavelet is available elsewhere [19].

Having introduced the wavelet transform, next is a brief description of the Walsh-Hadamard transform to complete the two constituents of the compression method proposed in this study for still images.

2.2. *Walsh-Hadamard Transform*

The Walsh-Hadamard transform of a sequence is expressible [20] as:

$$X_N = \frac{1}{N} H_N x_N \tag{8}$$

where H_N is a Hadamard matrix of order N and $x_N = \left[x_1, x_2, \cdots, x_N\right]^T$ represents an $N \times 1$ matrix. The Hadamard matrix of order N (where $N = 2^n$, n being a positive integer) is defined recursively by

$$H_N = \begin{bmatrix} H_{N/2} & H_{N/2} \\ H_{N/2} & -H_{N/2} \end{bmatrix} \tag{9}$$

where $H_1 = [1]$.

The Walsh-Hadamard transform can alternatively be expressed as:

$$X\left(u\right) = \frac{1}{N}\sum_{m=0}^{N-1} x\left(m\right)\left(-1\right)^{\langle m,u\rangle},\ u = 0,1,2,\cdots,N-1 \tag{10}$$

where

$$\langle m,u\rangle = \sum_{s=0}^{n-1} u_s m_s \tag{11}$$

and

$$n = \log_2 N \tag{12}$$

The terms u_s and m_s are the coefficients of the binary representations of u and m, respectively. The inverse of the Walsh-Hadamard transform is given by:

$$x(m) = \frac{1}{N}\sum_{m=0}^{N-1} X(u)(-1)^{\langle m,u\rangle},\ m = 0,1,2,\cdots,N-1 \tag{13}$$

3. METHOD

Figure 1 depicts the block diagram of the proposed compression scheme. Aside from the input and output stages, five other stages involved, are:

i. Conversion of the still image files into signal equivalent;
ii. Decomposition of the signal equivalent of the image file using bi-orthogonal wavelet transform;
iii. Further transformation of the decomposed version of the signal equivalent of the image file using Walsh-Hadamard transform to achieve compression;
iv. Obtaining compressed estimates of the original signal equivalent of an image file using inverse Walsh-Hadamard routine and
v. Application of inverse discrete wavelet transform routine on estimates obtained from inverse Walsh-Hadamard transform to reconstruct the compressed version of the image.

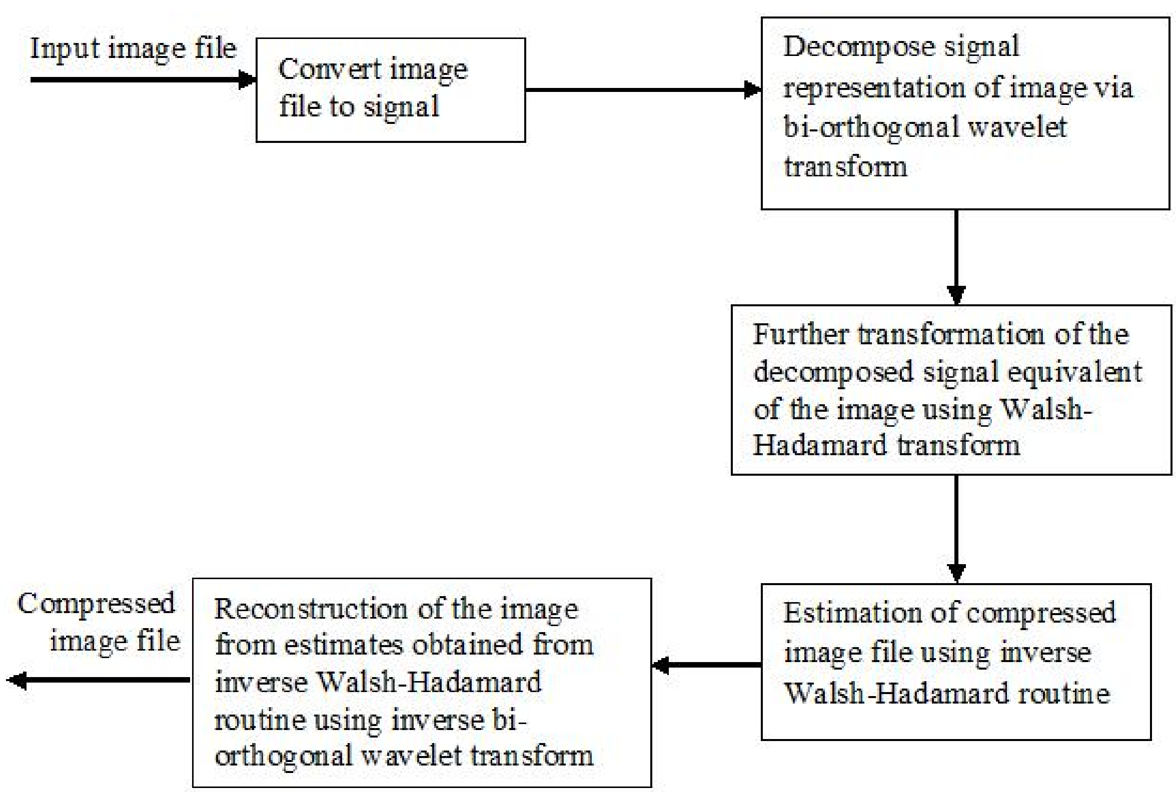

Figure 1: Block diagram of the proposed still image compression scheme

The first stage involves the conversion of the image file into an appropriate signal representation. This stage can be described as the pre-processing stage for the image file. The image file is read as input data and then converted into proper signal representation appropriate for decomposition by wavelet transform. Irrespective of the format in which the image file is prepared or saved, the file is opened, copied and saved into .jpg format. Files saved in .jpg format are read and converted into pixels. It is in this format that bi-orthogonal discrete wavelet transform decomposition is implemented. The image file's decomposed signal equivalent is then passed through the Walsh-Hadamard transform routine for further compression. The inverse Walsh-Hadamard routine is then invoked on the output. This is followed by inverse bi-orthogonal transform to reconstruct the compressed image from an ensemble of pixels equivalent. The proposed compression scheme was implemented in a MATLAB environment. It is worth noting that the decomposition level of two is used for bi-orthogonal wavelet transform, while Walsh-Hadamard of order two is equally employed.

Since the signal representation of an image file is a 2-D input signal, the application of discrete wavelet transform into such signal yields four output sequences: LL, LH, HL and HH sequences. The transform is easily realized by directly invoking finite impulse response convolution.

Consider a two-dimensional input signal $\mathbf{X}=\{x_{i,j}\}$, its discrete wavelet transform is implemented as

$$\{\mathbf{\Phi}_i\}=\frac{1}{\sqrt{2}}\sum_i a_k \,\mathrm{x}(2i+k) \tag{14}$$

$$\{\mathbf{\psi}_i\}=\frac{1}{\sqrt{2}}\sum_i (-1)^k a_{2N-1-k}\,\mathrm{x}(2i-k) \tag{15}$$

$$\{\mathbf{\Phi}_j\}=\frac{1}{\sqrt{2}}\sum_j a_k \,\mathrm{x}(2j+k) \tag{16}$$

$$\{\mathbf{\psi}_j\}=\frac{1}{\sqrt{2}}\sum_j (-1)^k a_{2N-1-k}\,\mathrm{x}(2j-k) \tag{17}$$

where N is a positive integer $k=1,2,\cdots 2N-1$ and a_k is a real number.

It should be noted that a total of fifteen variants of bi-orthogonal discrete wavelet transforms are selected and utilized in this work to decompose the signal representations of image files. The intuition behind this is to enable a systematic analysis of the performance of each of the bi-orthogonal wavelet variants for comparison purposes and consequent selection of the performing discrete filter for the actual compression task of still image file. The randomly selected discrete wavelet filters selected are 'biort1.1', 'biort1.3', 'biort1.5', 'biort2.2', 'biort2.4', 'biort2.6', 'biort2.8', 'biort3.1', 'biort3.3', 'biort3.5', 'biort3.7', 'biort3.9', 'biort4.4', 'biort5.5', and 'biort6.8').

Further transformation of the decomposed data string from the signal representation of the image file as output from discrete wavelet transform is done using the Walsh-Hadamard routine of order 2. The output of this stage yields a compressed data string representation of the image file. Furthermore, estimates of the compressed data string are obtained using the inverse Walsh-Hadamard routine, and the inverse discrete wavelet transform is carried out on the estimates (compressed data string) to reconstruct an approximate representation of the image file. It is worth noting that the compression scheme proposed in this work results from the integration of two lossy approaches (wavelet transform and Walsh-Hadamard transform). The fixed form soft thresholding scheme is used to estimate the error involved in the MATLAB implementation of the wavelet transformation of the signal representation of image files.

4. PERFORMANCE METRICS

Three standard metrics are used to evaluate the performance of the proposed image file compression scheme. They are: compression ratio (CR), mean square error (MSE) and peak signal-to-noise ratio (PSNR).

The compression ratio (CR) is defined as

$$CR = \frac{\textit{original image size}}{\textit{compressed image size}} \tag{18}$$

while the MSE is given by

$$MSE = \frac{1}{N}\sum_{n=1}^{N}\left(x_n - y_n\right)^2 \tag{19}$$

and the PSNR is expressible as

$$PSNR = 10\log\frac{x_{peak}^2}{MSE} \quad \text{dB} \tag{20}$$

where $\{x_n\}$ and $\{y_n\}$ represent the source signal sequence and reconstructed signal sequence, respectively, N is the number of elements in the sequence and x_{peak} is the peak signal value.

The data utilised in this paper are open-source images obtained from the Internet. Specifically, nine images of different sizes in kilobyte, are used. Table 1 presents details of the nine images, while Figure 2 depicts four of the images adopted in the experiment.

Table 1: Original size of images employed in the analysis

Images	Size (Bytes)
1	196748
2	169425
3	116107
4	115725
5	786572
6	886706
7	131084
8	77842
9	20949

(a) (b) (c) (d)

Figure 2: Specimen images used for the experimentation of the developed image compression scheme (a) image 3 (b) image 4 (c) image 8 (d) image 9

4. RESULTS AND DISCUSSION

Evaluation of the output of the formulated and implemented image compression scheme involving each of the fifteen DWT variants using the nine images above is required. It is necessary to isolate and select the most suitable bi-orthogonal discrete wavelet function that performs best about the metrics adopted for this research. Each of the fifteen bi-orthogonal discrete wavelet function variants selected experiments using the nine different images whose sizes are shown in Table 1. Table 2 gives the numerical values of the computed compression ratio from the experiments.

Table 2: CR resulting from the experimentation of the proposed compression scheme and the corresponding DWT variants employed

DWT	Experiments								
Variants	1	2	3	4	5	6	7	8	9
biort1.1	18.03	1.73	1.42	1.46	17.99	11.37	1.41	1.01	1.15
biot1.3	15.87	1.60	1.29	1.33	17.09	10.59	1.25	0.91	1.05
biot1.5	15.56	1.58	1.32	1.33	15.72	10.42	1.28	0.96	1.07
biort2.2	15.41	1.63	1.39	1.43	17.19	12.36	1.36	1.12	1.22
biort2.4	15.58	1.67	1.39	1.43	17.13	12.03	1.38	1.14	1.21
biort2.6	13.86	1.54	1.29	1.33	15.52	11.78	1.31	1.07	1.18
biort2.8	13.91	1.59	1.31	1.35	15.40	11.42	1.32	1.12	1.19
biort3.1	15.44	1.58	1.35	1.37	17.20	12.33	1.34	1.18	1.19
biort3.3	12.64	1.55	1.35	1.35	14.83	11.69	1.28	1.17	1.21
biort3.5	12.69	1.61	1.33	1.35	13.83	11.68	1.32	1.13	1.20
biort3.7	11.62	1.50	1.23	1.26	13.27	11.12	1.24	1.16	1.16
biort3.9	11.81	1.44	1.25	1.25	12.81	11.25	1.27	1.09	1.13
biort4.4	17.20	1.78	1.51	1.53	19.07	13.71	1.49	1.16	1.38
biort5.5	18.98	1.93	1.67	1.67	20.10	14.47	1.65	1.22	1.45
biort6.8	15.80	1.68	1.42	1.46	16.97	12.80	1.41	1.14	1.30
Average	14.96	1.63	1.37	1.39	16.27	11.93	1.35	1.11	1.21

Results presented in Table 2 reveal that the DWTs variant exhibits varying patterns concerning compression ratio in the nine experiments. The lowest compression ratio recorded is 11.62 corresponding to biort3.7 (for experiment 1); 1.50 when biort3.7 is used (in experiment 2); 1.23 associated with biort3.7 (in experiment 3); 1.25 corresponding to biort3.9 (in experiment 4); 12.81 for biort3.9 (in experiment 5); 10.42 for biort1.5 (in experiment 6); 1.24 for biort3.7 (in experiment 7); 0.91 for biort1.3 (in experiment 8) and 1.05 biort1.3 (in experiment 9). The highest values of recorded CR are 18.98, 1.93, 1.67, 1.67, 20.10, 14.47, 1.65, 1.22, and 1.45 for biort5.5 in experiments 1 – 9.

For each of the experiments, the class average is computed. Computed class averages of CR are 14.96, 1.63, 1.37, 1.39, 16.27, 11.93, 1.35, 1.11 and 1.21 for experiments (images) 1-9, respectively. From the computed class averages, bi-orthogonal DWT variants employed are pruned down using a DWT variant having a value of CR greater or equal to the class average as a criterion. Consequently, DWTs that return values of less than the class average in an experiment is dropped. Thus, DWT variants that met the criterion for each of the experiments are:
Image 1: biort1.1, biort1.3, biort1.5, biort2.2, biort2.4, biort3.1, biort4.4, biort5.5, biort6.8
Image 2: biort1.1, biort2.2, biort2.4, biort4.4, biort5.5, biort6.8
Image 3: biort1.1, biort2.2, biort2.4, biort4.4, biort5.5, biort6.8
Image 4: biort1.1, biort2.2, biort2.4, biort4.4, biort5.5, biort6.8
Image 5: biort1.1, biort1.3, biort2.2, biort2.4, biort3.1, biort4.4, biort5.5, biort6.8
Image 6: biort2.2, biort2.4, biort3.1, biort4.4, biort5.5, biort6.8
Image 7: biort1.1, biort2.2, biort2.4, biort4.4, biort5.5, biort6.8
Image 8: biort2.2, biort2.4, biort2.8, biort3.1, biort3.3, biort3.5, biort3.7, biort4.4, biort5.5, biort6.8
Image 9: biort2.2, biort2.4, biort3.3, biort4.4, biort5.5, biort6.8

It can be inferred that only five DWT variants, biort2.2, biort2.4, biort4.4, biort5.5 and biort6.8 have C.R. values equal or greater than the respective class averages. They are, therefore, selected for further analysis while the remaining DWT variants are dropped.

Presented in Table 3 are computed mean square error (MSE) linked to the utilization of the five DWT variants that fulfil the CR selection criterion for the nine experiments. In contrast, Table 4 shows the corresponding peak signal-to-noise ratio (PSNR). Regarding MSE, DWT variants with the lowest MSE figure are considered better. Out of the five remaining DWTs under consideration, the lowest MSE figures are 244.28 with biort2.2 (experiment 1); 428.63 with biort2.4 (experiment 2); 190.34 with biort2.4 (experiment 3); 247.33 using biort2.2 (experiment 4); 208.23 using biort2.2 (experiment 5); 350.38 using biort2.4 (experiment 6); 284.09 with biort2.2 (experiment 7); 401.90 with biort2.2 (experiment 8) and 120.87 with biort2.2 (experiment 9).

Table 3: MSE obtained from the experiment using the proposed compression scheme and the corresponding DWT variants employed

DWT Variants	Experiments								
	1	2	3	4	5	6	7	8	9
biort2.2	244.28	431.38	194.09	247.33	208.23	393.11	284.09	401.90	120.87
biort2.4	277.96	428.63	190.34	251.73	216.26	350.38	286.31	446.60	128.12
biort4.4	305.47	448.51	208.21	276.12	252.31	385.00	309.30	475.89	152.27
biort5.5	309.99	513.48	261.10	333.00	339.82	524.21	368.09	502.18	201.00
biort6.8	285.92	450.22	214.63	274.62	272.56	429.22	305.50	423.00	151.64

A cursory look at entries of Table 3 shows that the compression scheme employing biort2.2 has the lowest MSE values when images 1, 4, 5, 7, 8 and 9 are used, while for images 2, 3 and 6, the compression scheme involving biort2.4 return the lowest MSE figures in each case of the three experiments. One thing that can be deduced from this experiment is that, although the values of computed CR of compression scheme using biort2.2 and biort2.4 are lower than those of biort4.4, biort5.5 and biort6.8, the two DWT variants (biort2.2 and biort2.4) are better in terms of MSE values.

Next, the PSNR figures resulting from biort2.2, biort2.4, biort4.4, biort5.5 and biort6.8 in the construction of compression schemes are evaluated. Table 4 presents results obtained from computations. A close observation of entries of Table 4 shows that the highest PSNR values when images 1, 4, 5, 7, 8 and 9 serve as input are recorded when biort2.2 is used in the implementation of the image compression scheme, while for images 2, 3 and 6, compression scheme involving biort2.4 returns the highest PSNR values. Values of PSNR obtained from implementations employing biort4.4, biort5.5 and biort6.8 are lower than the highest value in each of the nine experiments.

Table 4: PSNR resulting from the experimentation of the proposed compression scheme and the corresponding DWT variants employed

DWT Variants	Experiments								
	1	2	3	4	5	6	7	8	9
biort2.2	72.38	69.91	73.38	72.33	73.08	70.32	71.73	70.22	75.44
biort2.4	71.82	69.94	73.47	72.25	72.91	70.82	71.69	69.76	75.19
biort4.4	71.41	69.74	73.08	71.85	72.24	70.41	71.36	69.49	74.44
biort5.5	71.35	69.16	72.09	71.04	70.95	69.07	70.60	69.25	73.23
biort6.8	71.70	69.73	72.94	71.87	71.91	69.93	71.41	70.00	74.45

From the preceding, it is evident that the compression scheme implementing biort2.2 is associated with the lowest values of MSE and highest values of PSNR in six out of the nine experiments, while implementation employing biort2.4 recorded the lowest MSE figure and highest PSNR values in the remaining three experiments. This suggests that the pendulum of best bi-orthogonal DWT variants considered in this research for implementing the image compression scheme oscillates between biort2.2 and biort2.4. The difference between MSE figures recorded by compression scheme implementation involving biort2.2 concerning those obtained when biort2.4 is used are 0.64% (experiment 2), 1.97% (experiment 3), and 12.20% (experiment 6).

Similarly, the corresponding difference in PSNR figures is 0.04% (experiment 2), 0.12% (experiment 3), 0.71% (experiment 6). Without loss of generality, it is evident that the compression scheme implemented with biort2.2 appears better in all nine experiments than that involving biort2.4, according to the results of the analysis carried out in this research. The compressed file sizes determined for each of the resultant two compression schemes involving biort2.2 and biort2.4 concerning the nine sets of experimental simulations are shown in Table 5. The values of compressed image sizes resulting from the nine experiments are revealing. While implementing biort2.2 yields the lowest compressed image size in experiments 3, 5, 6 and 9, the compression scheme implemented with biort2.4 yields the lowest compressed image sizes in experiments 1, 2, 4, 7 and 8. The difference in compressed file sizes recorded by the compression scheme implementing biort2.2 concerning implementing biort2.4 in percentages are 1.12% (experiment 1), 2.73% (experiment 2), 0.02% (experiment 4), 2.01% (experiment 7) and 1.99% (experiment 8).

It is clear from the above analysis that the relative advantage of reduced compressed image sizes, recorded by implementation involving biort2.4 over the compression scheme employing biort2.2, is marginal, the highest being 2.73% in experiment 2. Therefore, implementing biort2.2 in its construction without loss of generality is better than biort2.4. This is premised on the values of MSE and PSNR computed for biort2.2 DWT used in the construction. Thus, it can be safely said that the compression scheme formulated with a combined Walsh-Hadamard transform and discrete wavelet transform (biort2.2 variant) is the best-suited combination for the image compression scheme among the selected bi-orthogonal discrete wavelet transform functions.

Table 5: Compressed image sizes (kB) from the experiments

DWT Variants	Experiments								
	1	2	3	4	5	6	7	8	9
biort2.2	12770	103992	83583	81042	45764	71754	96694	69346	17126
biort2.4	12629	101231	83775	81029	45920	73736	94787	67995	17292

5. CONCLUSION

Based on the results obtained in this research, the combined Walsh-Hadamard transform and bi-orthogonal wavelet transform could be employed to formulate high-performing image compression schemes. Depending on the adopted wavelet transform functions, compression schemes of varying performance, in terms of compression ratio, mean square error and peak signal-to-noise ratio, are realizable. Therefore, by carefully selecting performance indicators, image compression schemes of different grades can be formulated from combined Walsh-Hadamard and bi-orthogonal transforms. For the fifteen different bi-orthogonal wavelet transform functions ('biort1.1', 'biort1.3', 'biort1.5', 'biort2.2', 'biort2.4', 'biort2.6', 'biort2.8', 'biort3.1', 'biort3.3', 'biort3.5', 'biort3.7', 'biort3.9', 'biort4.4', 'biort5.5', and 'biort6.8') employed along with Walsh-Hadamard function, in the formulation of still image compression schemes in this research, bi-orthogonal transform variant 2.2 (biort2.2) performed best. This is stem from the obtained
values for compression ratio, mean square error and peak signal-to-noise ratio.

REFERENCES

[1] Jayasankar U., V. Thirumal and D. Ponnurangam. 2021. A survey on data compression techniques: From the perspective of data quality, coding schemes, data type and applications, *Journal of King Saud University - Computer and Information Sciences*, 33(2):119–140.

[2] Rahman A. and M. Hamada. 2019. Lossless Image Compression Techniques: A State-of-the-Art Survey, *Symmetry (Basel)*, 11(10):1274. doi: 10.3390/sym11101274.

[3] Al-jawaherry M.A., and S.Y. Hamid. 2021. Image compression techniques: literature review. *Journal of Al-Qadisiyah for Computer Science and Mathematics*, 13(4):10-21.

[4] Kharate G.K. and V.H. Patil. 2010. Color Image Compression Based On Wavelet Packet Best Tree, *Int. J. Comput. Sci. Issues*, 7(2):31–35, 2010.

[5] Pabi D.J.A., N. Puviarasan and P. Aruna. 2017. Fast Singular value decomposition based image compression using butterfly particle swarm optimization technique (SVD-BPSO)," *Int. J. Comput. Eng. Res. Trends*, 4(4):128–135.

[6] Kong S., L. Sun, C. Han, and J. Guo. 2017. An image compression scheme in wireless multimedia sensor networks based on NMF, *Inf.*, 8(1):1–14. doi: 10.3390/info8010026.

[7] Kumar R., U. Patbhaje, and A. Kumar. 2019. An efficient technique for image compression and quality retrieval using matrix completion, *J. King Saud Univ. - Comput. Inf. Sci.*, doi: 10.1016/j.jksuci.2019.08.002.

[8] Li S. and L. Jia. 2019. Rate Allocation with Near-optimal Rate-distortion Performance for JPEG-LS, *Tenth Int. Conf. Signal Process. Syst.*, 11071(110710M). doi: 10.1117/12.2521483.

[9] Jeromel A. and B. Zalik. 2020. An efficient lossy cartoon image compression method," *Multimed. Tools Appl.*, 79:433–451. Available: https://doi.org/10.1007/s11042-019-08126-7.

[10] Petö M., F. Duvigneau, and S. Eisenträger. 2020. Enhanced numerical integration scheme based on image-compression techniques: application to fictitious domain methods," *Adv. Model. Simul. Eng. Sci.*, 7(21). doi: 10.1186/s40323-020-00157-2.

[11] Wang J., M. Terpstra, J. Kosinka, and A. Telea. 2020. Quantitative evaluation of dense skeletons for image compression," *Inf.*, 11(5):1-18. doi: 10.3390/INFO11050274.

[12] Al-khassaweneh M. and O. Al-Shorman. 2020. Frei-Chen bases based lossy digital image compression technique image, *Appl. Comput. Informatics*. https://www.emerald.com/insight/2210-8327.htm%0AFrei-Ch.

[13] Lone M.R. 2020. A high speed and memory efficient algorithm for perceptually-lossless volumetric medical image compression, *J. King Saud Univ. - Comput. Inf. Sci.*, no. xxxx, 2020, doi: 10.1016/j.jksuci.2020.04.014.

[14] Mustafa, R., Ahmedi, B., and Mustafa, K. 2021. Compression of Monochromatic and Multicolored Image with Neural Network. *Asian Journal of Research in Computer Science*, *9*(1):39–45. https://doi.org/10.9734/ajrcos/2021/v9i130213

[15] Zhang Y., J. Jiang, and G. Zhang. 2021. Compression of remotely sensed astronomical image using wavelet-based compressed sensing in deep space exploration, *Remote Sens.*, 13(2):1–16. doi: 10.3390/rs13020288.

[16] Ko H.H. 2021. Enhanced binary MQ arithmetic coder with look-up table," *Inf.*, 12(4). doi: 10.3390/info12040143.

[17] Svynchuk O., O. Barabash, J. Nikodem, R. Kochan, and O. Laptiev. 2021. Image compression using fractal functions," *Fractal Fract.*, 5(2):1–14. doi: 10.3390/fractalfract5020031.

[18] Amusa K.A., A. Adewusi, T.C. Erinosho, S.A. Salawu, D.O. Odufejo. 2022. On the Application of Wavelet Transform and Huffman Algorithm to Yorùbá Language Syntax Text Files Compression. Serbian Journal of Electrical Engineering 19(3):351-368. https://doi.org/10.2298/SJEE2203351A

[19] Feauveau J.C., A. Cohen, I. Daubechies: 1992. Bi-orthogonal bases of compactly supported wavelets, *Communications on Pure and Applied Mathematics*, 45(5):485–560.

[20] Kondamuri S.R. and S. Anuradha. 2020. Walsh-Hadamard-transform-based SC-FDMA System using WARP hardware. *ETRI Journal,* 43(2):197–208. https://doi.org/10.4218/etrij.2019-0502